Holographic Polymer-Dispersed Liquid Crystals and Polymeric Photonic Crystals Formed by Holographic Photolithography

Thein Kyu*, Scott Meng, Hatice Duran, Kumar Nanjundiah, and Gregory R. Yandek

Department of Polymer Engineering, University of Akron, Akron, OH 44325-0301

Abstract: The present article describes the experimental and theoretical observations on the formation of holographic, polymer-dispersed, liquid crystals and electrically switchable, photonic crystals. A phase diagram of the starting mixture of nematic liquid crystal and photo-reactive triacrylate monomer was established by means of differential scanning calorimetry (DSC) and cloud point measurement. Photolithographic patterns were imprinted on the starting mixture of LC/triacrylate via multi-beam interference. A similar study was extended to a dendrimer/ photocurative mixture as well as to a single component system (tetra-acrylate). Theoretical modeling and numerical simulation were carried out based on the combination of Flory-Huggins free energy of mixing and Maier-Saupe free energy of nematic ordering. The combined free energy densities were incorporated into the time-dependent Ginzburg-Landau (Model C) equations coupled with the photopolymerization rate equation to elucidate the spatio-temporal structure growth. The 2-D photonic structures thus simulated were consistent with the experimental observations. Furthermore, 3-D simulation was performed to guide the fabrication of assorted photonic crystals under various beam-geometries. Electro-optical performance such as diffraction efficiency was evaluated during the pattern photopolymerization process and also as a function of driving voltage.

Keywords: polymer-dispersed liquid crystals, photonic crystals, photolithographic.

Introduction

Photonic crystals are dielectric substances with periodic structures that are structured to exhibit photonic band gap characteristics.[1,2] Depending on the size and structure of the periodic spacing, propagation of light is prohibited in a certain range of frequencies. Conventional photonic materials take advantage of structures possessing a high dielectric constant contrast with air, targeted at potential applications in optical computers and telecommunication, analogous to their silicon counterpart in information technology.[3,4]

Among many fabricating techniques for photonic crystals, holographic lithography (or pattern photo-polymerization) is a preferred method by virtue of its fast and easy processing capabilities.[5,6] Basically, holographic lithography technique operates based on the principles of multi-beam optical interference in creating 1-dimensional and multi-dimensional periodic interference patterns with alternating low intensity and high intensity regions. These photo-patterns are imprinted onto the mixtures of photo-curable monomers and another component to produce photonic crystals. Classified by the periodicity, holographic polymer dispersed liq-uid crystals may be categorized into a class of 1-D photonic crystals. In the fabrication of holographic polymer dispersed liquid crystal (H-PDLC), nematic liquid crystal (LC) has been commonly used as a second component so that the LC directors may be switched under the external electric voltage.[7] Although the dielectric contrast in the H-PDLC might be comparatively small, the electrical switchability makes such H-PDLC materials unique.

Recent progress in H-PDLC has been contributed primarily by Bunning et al.[8,9] as well as Crawford et al.[10] who conducted extensive studies on the transmission and reflection H-PDLC gratings and concomitant evaluation of electro-optical performance as a function of monomer functionality, LC composition, spacing, and starting temperature, among others. While the experimental findings in H-PDLC are well documented, there are limited efforts in the theoretical elucidation of the development of H-PDLC morphology.[11] Particularly, the correlation between the emerged morphology and the electro-optical performance has been missing in literature. Sutherland et al. are the first to demonstrate theoretically the relationship between the H-PDLC structural development of homogenous grating to the temporal evolution of diffraction efficiency.[12] Based on a rigorous pattern formation approach combined with the coupled wave theory

*Corresponding Author. E-mail: tkyu@uakron.edu

and Fourier approach, Meng *et al.* extended the aforementioned methodology to the gratings containing inhomogenous stripes, i.e., a step closer to the experimental observation.[13]

In this paper, various photocurable acrylate monomer/E7 liquid crystal mixtures were utilized for photolithography experiments with emphasis on the fabrication and characterization of multi-dimensional photonic crystals and their corresponding electro-optical properties. The resultant photonic structures have been characterized by polarized optical microscopy, atomic force microscopy, and time-resolved small angle light scattering equipped with a 2-D detector. In the subsequent study, the second component E7 has been replaced with a dendrimer to explore possible sensor applications. It will be further demonstrated that multi-dimensional photonic crystal can be made in a single component system of photo-curable monomer. The electrical switching characteristics of the aforementioned H-PDLC have also been investigated.

To gain in-depth understanding of thermodynamic and kinetic phenomena governing the spatio-temporal evolution of the H-PDLC and photonic structures, theoretical modeling and numerical simulation have been undertaken through incorporation of Flory-Huggins free energy of isotropic mixing and Maier-Saupe free energy of nematic ordering into the time-dependent Ginzburg-Landau (Model C) equations, coupled with the photo-polymerization reaction kinetic equation. The numerical simulation based on two and four-beam configurations revealed striking similarity between the theoretical predictions and experimental observations in respects of patterns, length and time scales. The effects of beam configuration on the final morphology of photonic crystals have been demonstrated including a face-centered cubic (FCC) lattice structure. Eventually, the switching of diffraction efficiency of H-PDLC, an important electro-optical property, has been experimentally tested and the results are well interpreted by the aforementioned model developed upon the coupled wave theory and Fourier approach.[13]

Theoretical Background

The holographic pattern formation in mixtures of photo-reactive monomer and nematic liquid crystal subjected to pattern photopolymerization may be modeled in the framework of the time-dependent Ginzburg-Landau equations (TDGL, Model C) with a conserved compositional order parameter, ϕ and a non-conserved orientation order parameter, s coupled with photopolymerization reaction kinetics. The spatio-temporal evolution of the LC domains may be monitored via

$$\frac{\partial \phi_{LC}(\overset{r}{r},t)}{\partial t} = \nabla \cdot \left[\Lambda \nabla \left(\frac{\delta G}{\delta \phi_{LC}} \right) \right] \tag{1}$$

where $(\delta G/\delta \phi_{LC})$ represents the functional derivative of the total free energy with respect to the LC concentration, signi-

fying the pseudo-chemical potential of LC phase. Photopolymerization proceeds through the mechanism of free radical polymerization which may be incorporated in the formation of the stratified layers as

$$\frac{\partial \phi_m(\overset{r}{r},t)}{\partial t} = \nabla \cdot \left[\Lambda \nabla \left(\frac{\delta G}{\delta \phi_m} \right) \right] - k \left[1 + \nu \left(\cos \left(\frac{2\pi x}{L} N_x \right) \right. \right.$$
$$\left. \left. + \cos \left(\frac{2\pi y}{L} N_y \right) \right) \right] \phi_m \tag{2}$$

where k is the apparent reaction kinetic constant. N_x and N_y represent the number of periodic stripes in the x, and y direction on a square grid having a given lateral length L. The corresponding polymer concentration may be expressed as

$$\frac{\partial \phi_p(\overset{r}{r},t)}{\partial t} = \nabla \cdot \left[\Lambda \nabla \left(\frac{\delta G}{\delta \phi_m} \right) \right] + k \left[1 + \nu \left(\cos \left(\frac{2\pi x}{L} N_x \right) \right. \right.$$
$$\left. \left. + \cos \left(\frac{2\pi y}{L} N_y \right) \right) \right] \phi_m \tag{3}$$

The subscripts LC, m, and p signify liquid crystal, monomer, emerging polymer concentration, respectively. Λ is the mutual diffusion coefficient that obeys the Onsager reciprocal relationship.[11] By virtue of the cross-linking reaction, the mutual diffusion is essentially governed by the diffusions of residual monomer and LC as the emerged polymer chains are fixed at the chemical junction. That is to say, the anchored polymer chains may undergo Brownian motions locally, but will not involve in the mutual diffusion or transport.

Correspondingly, the orientation ordering of LC may be described in the non-conserved form as

$$\frac{\partial s(\overset{r}{r},t)}{\partial t} = -R_s \left(\frac{\delta G}{\delta s} \right) \tag{4}$$

where R_s is a constant that is related to the rotational mobility of the liquid crystal director. Needless to say, the pattern forming aspects in both the concentration and orientation fields is governed by the total free energy of the system G which may be described as

$$G = \int_V (g^i + g^n + \kappa_\phi |\nabla \phi|^2 + \kappa_s |\nabla s|^2) dV \tag{5}$$

where κ_ϕ and κ_s are the interfacial gradient coefficient of concentration and orientation, respectively. The local free energy in eq. (5) is further expressed in terms of the combination of Flory-Huggins free energy of isotropic mixing (g^i) and the Maier-Saupe free energy of nematic ordering (g^n). The FH free energy density of isotropic mixing for a binary mixture reads[14,15]

$$g^i = \phi_{LC} \ln \phi_{LC} / r_{LC} + (1 - \phi_{LC}) \ln \phi_{LC} / r_m + \chi \phi_{LC} (1 - \phi_{LC}) \tag{6}$$

where r_m and r_{LC} represent the statistical chain segment

156

lengths of polymer and liquid crystal molecules, respectively, which have been taken as: $r_m=3$ and $r_{LC}=1$ at the onset of polymerization. χ is the FH interaction parameter that takes the form of $\chi=A+B/T$ in which A and B are constants representing athermal entropic contribution and enthalpic contribution, respectively, and T the system's temperature.

The Maier-Saupe free energy of nematic ordering may be written as[16]

$$g^n = \frac{1}{r_{LC}}\left(-\phi_{LC}\ln z + \frac{1}{2}v\phi_{LC}^2 s^2\right) \tag{7}$$

where z is the partition function and v stands for the nematic interaction parameter taken as $v=4.541T_{NI}/T$, in which T_{NI} is the liquid crystal nematic-isotropic transition temperature. The orientation order parameter is defined as: $s = (3\angle \cos^2\theta > -1)/2$, θ being the angle between the LC director and the reference axis.

It should be emphasized that for a single component system of photocurable monomer, the total free energy may be described simply in the form of a Landau type[17]

$$g^i = \frac{r}{2}\phi_m^2 + \frac{u}{4}\phi_m^4 \tag{8}$$

where r and u are the coefficients having the same positive sign; otherwise eq. (8) represents a double well and thus represents a binary blend similar to the FH theory described by eq. (6). In the case of a single component system, eq. (8) may be modified as $g^i=(r/2)\phi_m^2$ with $r=1$ so that eq. (2) will reduce to the classical reaction-diffusion equation, i.e.,[18]

$$\frac{\partial\phi_m(\vec{r},t)}{\partial t} = \nabla\cdot\Lambda\nabla\phi_m - k\left[1+v\left(\cos\left(\frac{2\pi x}{L}N_x\right)\right. \right.$$
$$\left.\left. + \cos\left(\frac{2\pi y}{L}N_y\right)\right)\right]\phi_m \tag{9}$$

It should be cautioned that the above reaction-diffusion equation is only valid for a single component system since the free energy is of a single well type.

Phase Diagram Establishment. To establish the phase diagram, one of the essential criteria is that the chemical potential (μ) of each component of the system must be balanced in each phase. To determine the coexistence points of liquid-liquid phase separation in a binary fluid, the following conditions hold,

$$\mu_1(\phi_i^\alpha) = \mu_1(\phi_i^\beta) \text{ and } \mu_2(\phi_i^\alpha) = \mu_2(\phi_i^\beta) \tag{10}$$

where the superscripts α and β refer to respective coexisting phase, the subscripts 1 and 2 represent individual components, and the subscripts i and n denote the isotropic and nematic states. Alternatively, a double tangent method may be used to determine the binodal points as

$$\frac{[g^i(\phi_2^\alpha)+g^n(\phi_2^\alpha)]-[g^i(\phi_2^\beta)+g^n(\phi_2^\beta)]}{\phi_2^\alpha-\phi_2^\beta} = \frac{\partial(g^i+g^n)}{\partial\phi_2}\bigg|_{\phi_2=\phi_2^\alpha} \tag{11}$$

The solutions of eq. (11) under different temperatures render the phase diagram. The details of the double tangent method may be found elsewhere.[19]

Numerical Calculation Procedure. Eqs. (1-4) have been solved numerically on a 128×128 square lattice for 2-D simulation, or on a $128\times128\times38$ cubic lattice based on a finite difference method. A central difference discretization scheme was employed for the spatial step in conjunction with a forward difference discretization scheme for the time steps. In x and y directions, a periodic boundary condition was applied whereas no flux boundary condition was imposed in the thickness direction (z direction). The reference system for simulation is a multifunctional photo-reactive monomer (e.g., triacrylate, tetraacrylate) and nematic liquid crystal (e.g., E7). The diffusion coefficients for simulation are chosen to be in the range of the experimental diffusion coefficient for liquid crystal (i.e., 10^{-7}-10^{-8} cm^2/s) and for the multifunctional acrylic monomer (i.e., 10^{-10}-10^{-12} cm^2/s).

Experimental

The dispersing liquid crystal is a eutectic mixture of nematic liquid crystals, commercially known as E7 (EM Industries), consisting of various cyanobiphenyl (CB), oxycyanobiphenyl (OCB), and cyanoterphenyl (CT) derivatives in the following proportion: 5CB (51%), 7CB (21%), 8OCB (16%), and 5CT (12%) by weight. The nematic-isotropic transition of E7 is located at $T_{NI}=61\,^\circ$C with $\Delta H_{NI}=4.5$ J/g. The preference of choosing E7 is due to the broad nematic range (-30 to 61 °C) as opposed to a small gap of a few degrees for a single component liquid crystal, i.e., ~5 °C between the crystal-nematic transition and the nematic-isotropic transition (T_{NI}) for 5CB.

The multifunctional acrylate monomers selected for this study were difunctional monomers derived from ethoxylated bisphenol diacrylate (SR601, Sartomer Inc.), and pentaerythritol tetraacrylate from Aldrich. The dendrimer sample was synthesized in Prof. G. Newkome's lab.[20] These materials were used as received without further purification. The starting photoreactive syrup was prepared by mixing trimethylolpropane triacrylate as photoreactive monomer, a Rose Bengal derivative as photoinitiator, N-phenyl glycine (NPG) as co-initiator, N-vinyl pyrrolidone (NVP) as solubilizing agent, and octanoic acid as surfactant. The detailed formulation of the syrup may be found elsewhere.[18]

Regarding the establishment of phase diagrams, various E7/triacrylate mixtures were prepared by weighing various amounts of the constituents and subsequently stirring the mixtures at ambient temperature for 24 h. In the differential scanning calorimetry (DSC) experiment, thermal analyzer (Model Q1000, TA Instruments) equipped with a cooling

chamber was used in conjunction with liquid nitrogen as a purging and cooling medium. DSC experiments were performed in the temperature range of -40 to 70 °C to determine the nematic-isotropic transitions of the neat E7 and of its blends with multifunctional acrylate derivatives. The onset of nematic formation, corresponding to the DSC peak, was regarded as the nematic-isotropic transition temperature, T_{NI}. The T_{NI} of each mixture was then measured by repeating the heating and cooling cycles at the rates of 5, 3, and 2 °C/min. The transition temperature, T_{NI} was established in each case by extrapolating the recorded data of temperature to the zero rate.

A polarized microscope (Nikon Optipot 2-POL) equipped with a filtered Halogen light source was operated at 12 V and 100 W. A sample hot stage (Linkam Scientific Instruments, Model TS1500) was utilized in conjunction with a programmable temperature controller (Linkam, Model TMS93) and a cooling system (Model LNP93/2). The digital pictures were acquired using a Snappy interface/software at various magnifications of 100×~500×. The film thickness was controlled using a spacer of 20 μm.

Samples sandwiched between the glass slides and the cover glasses were heated at elevated temperature until the films became optically clear, and then were cooled down slowly at a natural rate. The samples were reheated to their isotropic states for 2 min to ensure that all samples received the same thermal history. The heating and cooling rate was 0.5 °C/min unless indicated otherwise. A temperature scan experiment was carried out for each composition from the isotropic temperature of the mixture by cooling it to ambient. The structural evolution of the biphasic domains was monitored by means of optical microscopy. In some instances when the microscopy technique was inconclusive, Fast Fourier transform (FFT) was carried out on the optical images to obtain light scattering patterns from which the cloud points may be determined. Since the process of phase separation is thermally reversible, the cloud point was measured by repeated heating and cooling cycles near the transition point.

The surface and bulk morphologies of the patterned H-PDLC samples were characterized by optical microscope and atomic force microscope (Quesant Instrument Corp. Model Q-scope 350). Subsequently, a two-dimensional light scattering device was employed for characterizing the diffraction patterns. The DE of transmission gratings was monitored using an Ocean Optics fiber-optic (operating range 350-1,000 nm with a resolution of ~1.5 nm) spectrometer. In the electro-optical switching, the H-PDLC films sandwiched between two indium-tin oxide (ITO) coated glass plates were placed normal to the direction of the laser beam (Ar ion laser with a wavelength of 532 nm). The transmitted and diffracted light intensities were measured under S-polarization and P-polarization using a photodiode. The grating was probed by means of a He-Ne laser (5 mW at 633 nm). The switching voltage versus transmission measurement of the H-PDLC film was

made under an electric field by bringing the read laser (He-Ne) at the Bragg angle while positioning the detector at the diffracted angle. A custom built amplifier/driver was utilized to generate the square waves at 1 kHz. The powers of the transmitted and the diffracted beams were measured as a function of applied electric field. The amplitude of the applied electric field was varied from 0 to 440 V across the films.

Results and Discussion

Establishment of Phase Diagrams of LC/Monomer Mixtures. The photo-polymerization was triggered by irradiating laser beam on the monomer syrup containing photoinitiators. Once the photo-polymerization starts, monomers get polymerized and the upper critical solution temperature (UCST) phase diagram of the starting mixture moves asymmetrically upward with increasing molecular weight, thrusting the system from the initial stable region into the unstable region. The final morphologies are strongly dependent on the initial location of the system in the starting phase diagram.[13] Hence, it is of utmost importance to establish a phase diagram of the starting monomer/LC, prior to the photo-patterning of acrylate/LC mixture. Figure 1 exhibits DSC thermograms, showing the nematic isotropic transitions of the E7 in its triacrylate blends. As evident in Figure 1, the nematic-isotropic transition temperature of pure E7 is located at 60 °C, but shows the depression trend with increasing monomer concentration. Neat E7 reveals a significantly sharper T_{NI} peak than those of its blends, i.e., the LC nematic-isotropic phase transition temperature peak broadens while the peak position moves to a lower temperature. The behavior of T_{NI} suppression suggests the possible miscibility or at least partial miscibility between the LC and triacrylate constituents. A similar behavior was observed in the tetraacrylate/E7 and pentaacrylate/E7 blends (data not shown). The cloud points were determined using the optical microscopy and/or
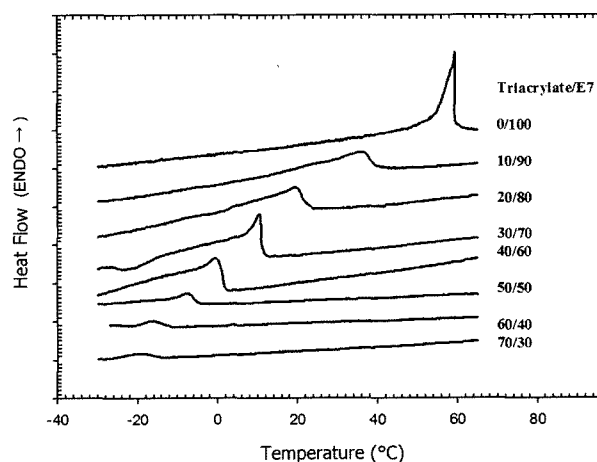

Figure 1. DSC thermograms of various triacrylate/E7 blends obtained at a cooling rate of 5 °C/min.

light scattering. The filled symbols in Figure 2 are experimentally measured points (or cloud points) from optical microscope and the open symbols from DSC. These results are in good accord in the high content LC regions; however, there is slight discrepancy between the points measured from DSC and those from optical microscope especially in the low LC content regions. It appears that DSC measures the transition temperature of the already phase separated LC domains whereas the cloud points represent the temperatures at which the first phase separated structure was detected. The close correspondence between the two data sets in the high LC content region suggests that the nematic–liquid transition line is close to the liquidus line in the high LC content regions. The deviation in the low LC content regions may be attributed to the possible existence of a UCST phase diagram at a lower temperature.

In Figure 2 is shown a theoretical coexistence curve constructed by solving eq. (6), (7), and (12) self-consistently based on the following conditions: $r_m=3$ and $r_{LC}=1$, and the critical temperature $T_c=256$ K. The constant A in the F-H interaction parameter was set arbitrarily as -11.8, which in turn yields $B=3015$ from the relationship, where $\chi_c=A+B/T_c$, is the critical interaction parameter, which may be estimated via the critical condition, $\chi_c = (\sqrt{r_{LC}}+\sqrt{r_m})^2 /2r_{LC}r_m$. The nematic-isotropic transition temperature was taken as $T_{NI}= 60\,°C$ for the reference nematic liquid crystal. Therefore, the nematic interaction parameter is determined in accordance with $\nu=4.541 T_{NI}/T$. The symbol I, N stand for isotropic and nematic region, respectively, with subscript m, n representing metastable, unstable regions. The dot-dash line represents the nematic-isotropic transition line and the dash line is the

nematic spinodal line. Between the coexistence curve and nematic spinodal line is the nematic metastable region. Encompassed by the nematic-isotropic transition line and nematic spinodal line is the nematic unstable region. The calculated coexistence curve conforms well to the cloud point data as well as the DSC results.

Photolithographic Patterning. As guided by the phase diagram, the starting acrylate/LC mixtures in the single phase region were selected and irradiated under the four-beam configuration of the holographic optical setup illustrated in Figure 3. The interference planes of the two-beams were orthogonal to each other but perpendicular to the sample plane. Figure 4 represents the AFM micrograph of the 35/65 E7/triacrylate mixture irradiated at 5 mW/cm² for 180 s. As can discerned in the periodicity profile, a submicron size-droplet array pattern was obtained with an average diameter of the individual droplet being 400~500 nm. Surface topology characterization by AFM shows a rectangular lattice consisting of non-sinusoidal peaks and valleys in which the valleys represent the areas where LC molecules reside.

After realizing the fabrication of switchable photonic crystal based on the acrylate/LC mixture, it is interesting to examine whether the same photolithographic technique is applicable to some systems containing different molecular architecture or longer chain length. The small molecule LC was replaced with a new class of material-called dendrimer. The chemical structures of the photocurable monomer and
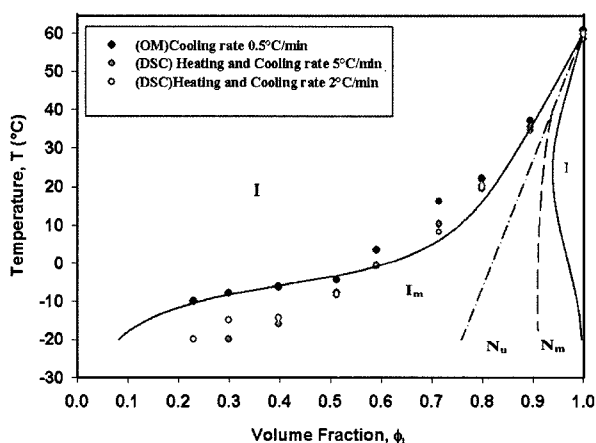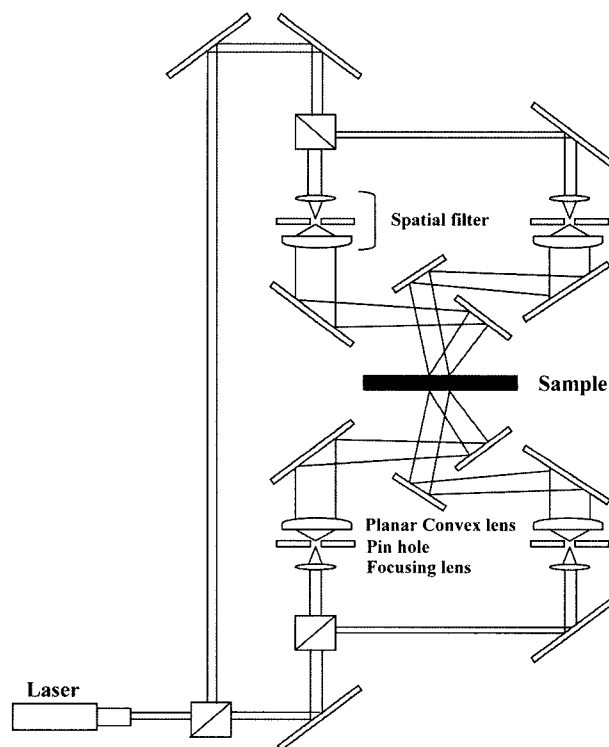
Figure 2. Experimentally determined phase diagram from cloud point and DSC measurements of the mixtures of triacrylate and E7 in comparison with the theoretically calculated curves in which the solid lines represent the coexistence curves, the dash line denotes the nematic spinodal, and the dot-dash line is the nematic isotropic transition. The coexistence regions were denoted by letters; I: stable isotropic region, I_m metastable isotropic, N: nematic region, N_u: unstable nematic, and N_m: metastable nematic regions.

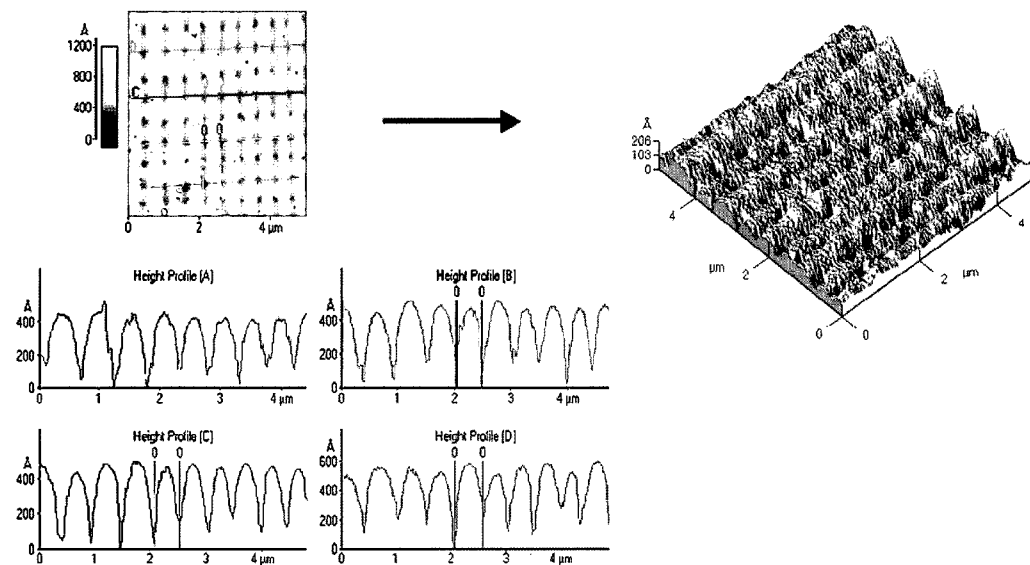**Figure 3.** Schematic representation of the multi-wave interference holographic technique.

Figure 4. AFM images of the micro-droplet patterns of the 35/65 E7/tetracrylate mixture fabricated via the 4-wave interference technique for 3 min radiation at 5 mW/cm². Upper left: 2-D surface profile, lower left: several spacing and films height values, Upper right: 3-D view of the micro-droplet pattern.
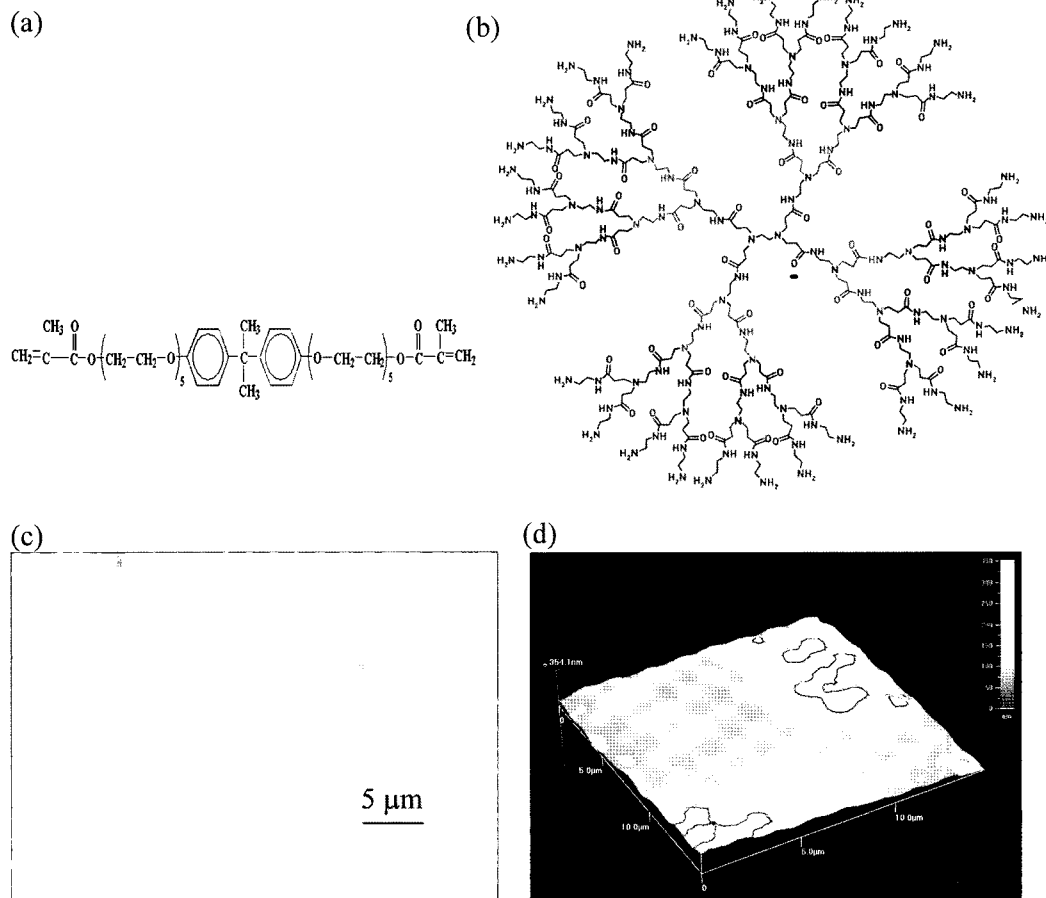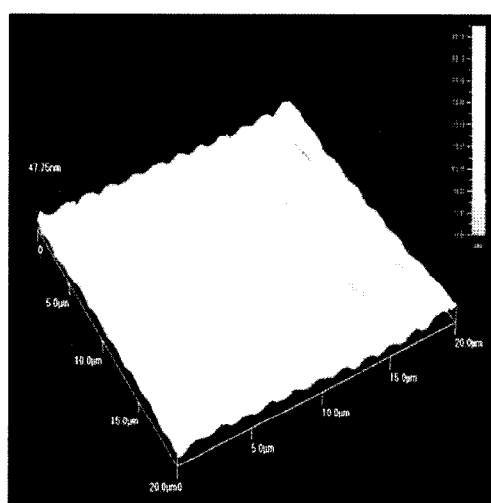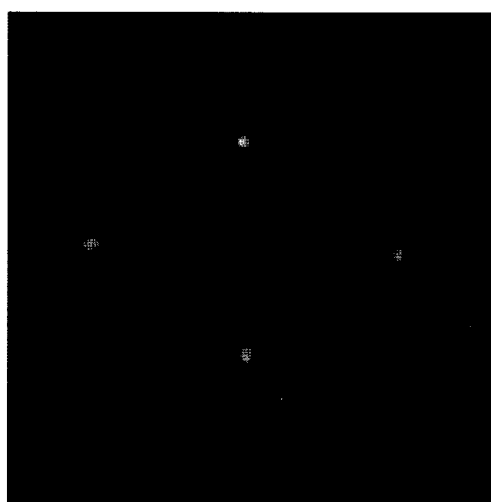

Figure 5. Chemical structures of (a) SR601 diacrylate monomer, (b) 16 arm dendrimer, (c) optical micrograph, and (d) AFM image of two dimensional photonic crystal photo-patterned in the mixture of SR601/dendrimer for 120 s.

dendrimer used in this study are illustrated in Figure 5(a) and (b), respectively. Figure 5(c) and (d) depicts the photonic crystal of the acrylate/16 arm dendrimer that were photo-polymerized for 120 s, showing a periodicity of 1.5 μm. With appropriate functional groups, such dendrimers may have potential use as sensors in pharmaceutical or biomedical applications. Although the application of the dendrimer based photonics or H-PDLC is still in its infancy, the proof-of-concept can now be established that the present methodology is not limited to small molecule LC, but may be applicable to larger macromolecular systems.

In addition, another attempt was made to photo-pattern a single component system such as a pure acrylic monomer. Figure 6(a) displays the AFM graph of the tetraacrylate

sample fabricated by 4-wave interference subjected to irradiation for 360 s. A micron-size droplet-array pattern was successfully created; the size of the individual droplet is about 2 μm. Further characterization of the sample in Figure 6(a) under the 2-D light scattering device reveals the two corresponding diffraction peaks in both the horizontal direction and vertical direction as depicted in Figure 6(b). The 2-D diffraction pattern suggests that the array pattern seen in Figure 6(a) is not a surface morphology, but it indeed represents the bulk concentration profile through the sample thickness.

To gain better understanding of the micro-void array pattern formation, a numerical simulation was also performed

(a) AFM micrograph: non-contact mode

(b) The corresponding diffraction pattern

Figure 6. (a) AFM graph of experimentally fabricated photonic structure from tetracrylate, showing micro-void array pattern irradiated for 360 s at 10 mW/cm² under 4-wave interference geometry, and (b) the corresponding diffraction patterns of the sample in Figure 6(a) obtained by time resolved 2-D light scattering.

1 0 0 0   1 0 0 0

4 0 0 0   4 0 0 0

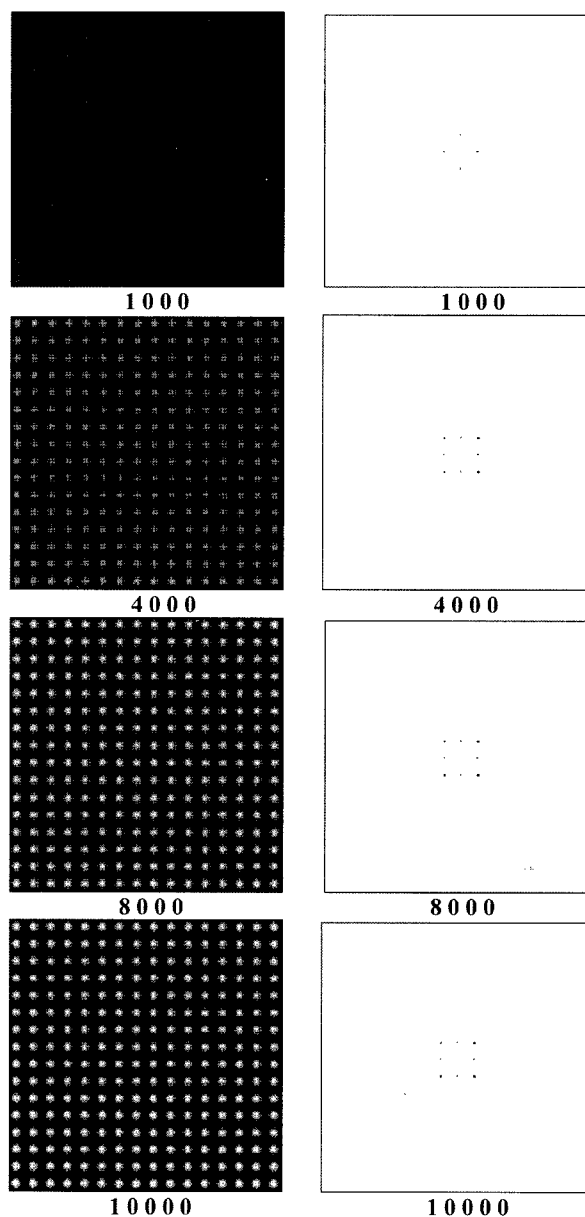8 0 0 0   8 0 0 0

1 0 0 0 0   1 0 0 0 0

Figure 7. Spatial temporal evolution of morphology in polymer concentration field showing micro-void array droplet patterns (left column), and corresponding Fourier transform patterns (right column).

in accordance with eqs. (2) and (8) under the conditions: N_x $=N_y=16$. The left column of Figure 7 illustrates the simulated spatio-temporal growth of the polymer concentration field. The formation of the micro-void array was discerned at 4,000 time steps. The average size of the simulated void is around 1~2 μm. With time progression to 10,000 time steps, the contrast in the polymer concentration with void (air) was enhanced without further structural transformation.

The corresponding Fourier transform patterns of the micro-void array patterns in Figure 7 are displayed in the right column. Initially the diffraction spots emerge both at the vertical and horizontal direction at 1,000 time steps similar to what was found experimentally in Figure 6(b). Later on, 4 additional diffraction spots emerged in the diagonal directions, indicating improved correlation in the diagonal direction of the micro-droplet array. The four diffraction spots in the diagonal region get intensified more at a later time steps of 8,000 to 10,000. Two possible scenarios may be envisaged for the lack of diagonal spots in the diffraction pattern; one possibility is that the experiment was terminated prematurely or needed longer exposure time. Another possibility may be due to the consequence of the poor incoherence length of the solid-state laser beam utilized in this particular experiment.

Three-Dimensional Photonic Crystals. One of the advantages of the holographic lithography technique is that photonic crystals of different lattice structure may be fabricated readily by simply changing beam configurations. In search of appropriate beam geometry, numerical simulation was carried out to guide the experimental fabrication of photonic crystal. It is apparent that the elastic free energy contribution from the emerging polymer network plays an important role on the final structure of H-PDLC materials. The elastic free energy for a flexible cross-linked polymer chain that obeys ideal Gaussian chain statistics may be described in accordance with the Dusek approach:[21]

$$g^e = \frac{3\alpha_e}{2r_c}\Phi_0^{2/3}(\phi_P^{1/3}-\phi_P)+\frac{\beta_e}{r_c}\phi_P\ln\phi_P \qquad (12)$$

where α_e and β_e are network constants. The term r_c is the segment length between cross-link points, which may be further expressed as a function of the monomer conversion, α, as[22]

$$r_c = \frac{\alpha}{2-\alpha-2\sqrt{1-\alpha}} \qquad (13)$$

It is evident that as the conversion increases, the segment length between crosslink points decreases, implying an increase in the crosslink density of the network.

Regarding the network constants in eq. (12), we have chosen the network parameters presented by Flory and Erman[23] in their junction fluctuation theory, allowing the constants to vary linearly with ϕ_P, which are defined as:

$$\alpha_e = (f-2)/f \ ; \qquad \beta_e = 2\phi/f \qquad (14)$$

where the parameter f denotes the functionality of the cross-links, taken as 3 in our calculations. The parameter Φ_0 in eq. (12), representing the reference volume fraction of the polymer network, is set to be equal to that at the onset of cross-linking $\Phi_0 = \phi_P$. This elastic free energy was added to the local free energy density of eq. (5) so that its contribution was accounted for during the time evolution calculation of the following 3D calculation.

Three-dimensional photonic crystals can be fabricated by irradiating the sample from both sides, employing the configurations comprised of four beams. One such arrangement, the two + two beam configuration, consists of two beams from the top together with two from the bottom. The two planes of the incident interference beams from the top and bottom are orthogonal to each other while the individual beams are directed from the opposite directions at some angles to the reflection plane that eventually determine the spacing of the periodic structures. The irradiance pattern resulting from this particular arrangement is described by the following equation[24]

$$\frac{I}{I_0} = 4\left[\cos^2\left(\frac{N_x}{L}x\right)+\cos^2\left(\frac{N_y}{L}y\right) \right.$$
$$\left. +2\cos\left(\frac{N_x}{L}x\right)\cos\left(\frac{N_y}{L}y\right)\cos\left(\frac{2N_z}{L}(z-h/2)\right)\right] \qquad (15)$$
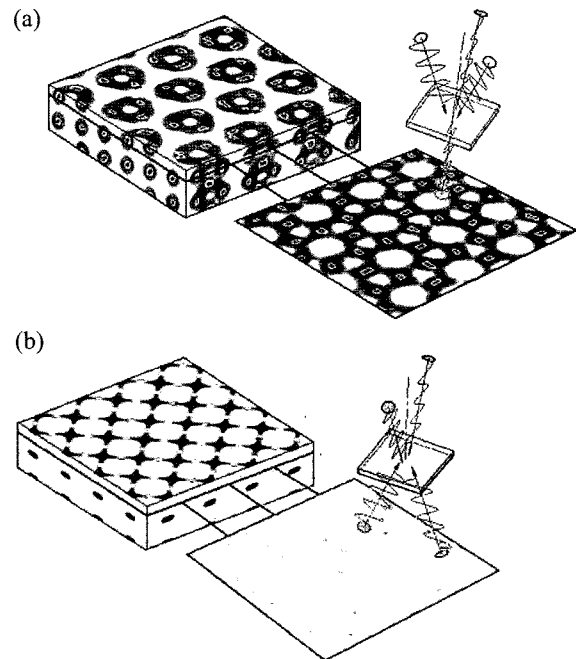
(a)

(b)

Figure 8. Simulated three dimensional photonic band-gap patterns under various multi-beam interference geometries including FCC (upper) and checker board patterns (lower) showing a 2D slice at a given depth.

where h represents the sample thickness. The resultant structure from this configuration is demonstrated in Figure 8(a), representing a snapshot at 4,500 time steps. This pattern may be characterized as a checkerboard type, with alternating layers of ellipsoidal shaped LC domains. To highlight the three-dimensional periodicity, a slice has been extracted from the lattice 375 nm from the top surface, exhibiting that the droplets are rotated $90°$ from those lying on the topmost layer.

The face-centered cubic (FCC) crystalline structure, which is well known to have the largest photonic band gap, may be created via a different photolithography configuration. The geometric arrangement of the beams in this case is the three-wave interference configuration from one side, with the addition of another beam irradiated on the sample, normal to the surface from the opposite side. The irradiance equation derived from this setup reads as follow:[24]

$$\frac{I}{I_0} = 4 + 2\left[\cos\left(\frac{2\sqrt{2}N_y}{9L}y\right)\cos\left(\frac{N_z}{9L}z\right)\right]$$
$$+ 2\left[\sin\left(\frac{2\sqrt{2}N_y}{9L}y\right)\sin\left(\frac{N_z}{9L}z\right)\right]$$
$$+ 4\left[\cos\left(\frac{\sqrt{6}N_x}{9L}x\right)\cos\left(\frac{\sqrt{2}N_y}{9L}y\right)\cos\left(\frac{N_z}{9L}z\right)\right] \qquad (16)$$
$$- 4\left[\cos\left(\frac{\sqrt{6}N_x}{9L}x\right)\sin\left(\frac{\sqrt{2}N_y}{9L}y\right)\sin\left(\frac{N_z}{9L}z\right)\right]$$
$$+ 4\left[\cos\left(\frac{\sqrt{6}N_x}{9L}x\right)\cos\left(\frac{\sqrt{2}N_y}{3L}y\right)\right] + 2\cos\left(\frac{2\sqrt{6}N_x}{9L}x\right)$$

The simulated morphology acquired at 4500 time steps is depicted in Figure 8(b) in conjunction with an extracted slice from the lattice 375 nm from the top surface. The peak (red) regions of the concentration profile denote high LC content, while the valleys (dark blue) represent areas low in LC. This particular structure has been recently fabricated experimentally from an initial mixture containing 36% LC content by weight, with LC droplets comparable in size to those obtained in our simulation.

Diffraction Efficiency and Switching Properties. The temporal growth of diffraction efficiency of the patterned structure may be monitored in-situ by applying the incident read beam (He-Ne) normal to the film and placing the photodiode at the angle of the first Bragg peak. Shown in Figure 9 is the real-time diffraction efficiency evolution of the acrylate/dendrimer sample in Figure 5. In principle, the diffraction efficiency is obtained by summing all diffraction peaks from the probe beam over the incident probe beam intensity. However, the intensity of the first Bragg peak is orders of magnitude stronger than those of the higher order peaks and thus only the first order peak was monitored in the present case. It is seen that almost 70% of the diffraction efficiency, as
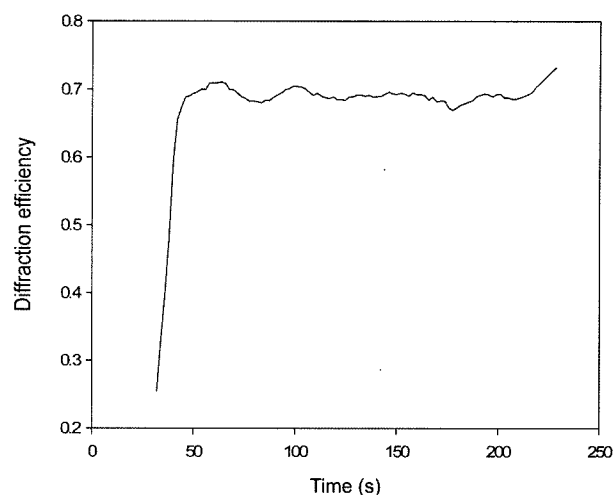

Figure 9. Temporal evolution of diffraction efficiency of the photonic structure shown in Figure 6.
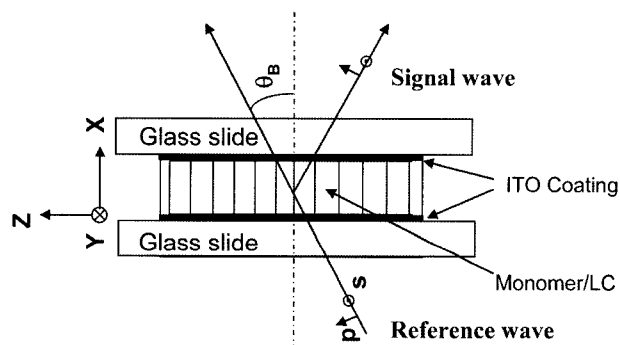

Figure 10. Schematic representation of switching of a transmission grating.

monitored from the first order Bragg peak, was achieved in less than 50 s. Subsequently, the diffraction efficiency levels off asymptotically. This diffraction efficiency development manifests the formation of the periodic striations having dielectric contrasts.

The electro-optical switching performance was evaluated in S- and P-polarization configurations of the transmission grating; its experimental electro-optical geometry is illustrated in Figure 10. The liquid crystal/monomer mixtures were sandwiched between the two ITO coated glass slides. The transmission grating layers were formed from these liquid crystal/monomer mixtures by bringing the two writing interference beams on one side of the sandwiched assembly such that the alternating layers form in perpendicular to the glass slides. The probed beam (He-Ne) was incident at a Bragg angle to the H-PDLC assembly layers, and the diffraction intensity was measured in the P-polarization (in plane) and the S-polarization (out-of-plane, i.e., normal to the plane of polarization of the incident beam). In this experi-

ment, the diffraction efficiency (DE) of the H-PDLC samples containing 40% LC was measured by taking the ratio of the first diffracted peak intensity relative to the overall intensity as a function of driving voltage. The detailed description of the electro-optical configuration for transmission gratings may be found elsewhere.[25]

Electro-optical response measurements of the H-PDLC films were performed at the first Bragg angle so that the applied electric field does not interfere with the probed He-Ne laser. Figure 11 exhibits the variations of diffraction efficiency in the S- and P-polarizations in the transmission grating of the 60/40 triacrylate/LC by applying various AC voltages at 1 kHz. The diffraction efficiency at S-polarization in the transmission grating diminishes asymptotically to a minimum at the applied voltage of ~20 V/μm (Figure 11(a)). The P-polarization, on the other hand, first exhibits a finite DE value in the off-state, then it declines to a minimum at ~17.5 V/μm, but shows a slight up-turn with continued
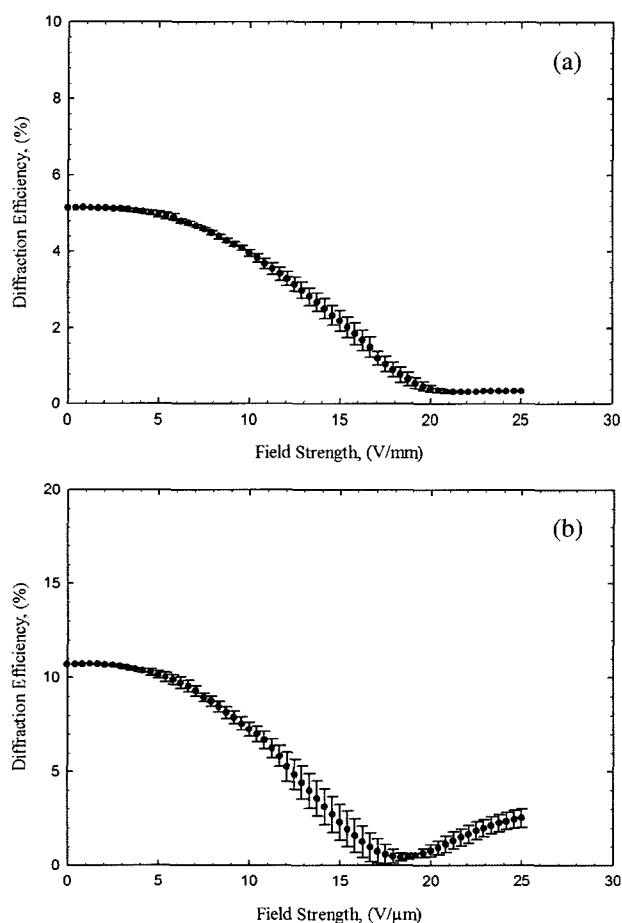

Figure 11. Electrical switching characteristics of the 60/40 triacrylate/LC mixture showing the diffraction efficiency grating as a function of driving voltage in the (a) S-polarization and (b) P-polarization. The samples were prepared by two-wave interference under irradiation at 5 mW/cm^2 intensity for 30 s. The curves were the average of 3 runs.

increase of the applied voltage (Figure 11(b)).

The above diffraction efficiency behavior may be explained in the context of a theoretical relationship that links the diffraction efficiency to the refractive index modulation in relation to the LC director orientation.[13] In the transmission grating, the diffraction efficiency for S-polarization is given as

$$\eta = \delta_a \, \sin^2\!\left(\frac{\pi \Delta n_j(t) l}{\lambda \cos \theta_B}\right) \qquad (j = s, p) \tag{17}$$

where δ_a is a correction factor for the scattering arising from the structural heterogeneity, l is the sample thickness, λ is the wavelength of the probe beam and θ_B the Bragg angle. In eq. (17), $\Delta n_j(t)$ is the refractive index modulation. Physically, $\Delta n_s(t)$ is a measure of the refractive index contrast between the stripe in the high intensity region and low intensity region along the y-direction, whereas $\Delta n_p(t)$ the refractive index contrast between refractive index modulation in the z- and x-directions. The detailed description of the model may be found in an earlier paper.[13]

In the H-PDLC layers, there exists a refractive index contrast between the z-axis and x-axis prior to the switching experiment. Although LC molecules are highly anisotropic having a large dielectric anisotropy, the power of the laser is sufficiently strong to orient the LC directors in perpendicular to the polarization direction of the incident beam. Hence, some component of the dielectric constants (refractive indices) arising from the LC molecules resided within the acrylate/LC inhomogeneous stripes would align preferentially along the z-axis (i.e., the grading direction), while some would orient in the x-direction. As illustrated in Figure 10, when the electric voltage is applied along the x-axis, the LC directors align more with their long axis (i.e. extraordinary refractive index) toward the field direction. The ordinary refractive index of the LC directors would match with the refractive index of the matrix polymer in the y-direction (i.e., perpendicular to the plane of polarization or S-polarization). As a result, the diffraction efficiency in the S-polarization gradually drops off and eventually diminishes with increasing driving voltage due to the increased LC director orientation toward the external electric field direction. On the other hand, this applied electric field would suppress the refractive index modulation in the z-direction. Hence, the refractive index contrast is reduced in the P-polarization, causing the diffraction efficiency to decline to a minimum. However, with further increase of the electric field, the refractive index modulation in the x-axis exceeds that in the z-direction; thereby the P-polarized DE starts to increase again. It may be inferred that the electrical switching of the H-PDLC can be performed from the off-state (0 V) to the on-state (20 V/μm for the grading along the S-polarization and 17.5 V/μm for the P-polarization).

References

(1) E. Yablonovitch, *Phys. Rev. Lett.*, **58**, 2059 (1987).

(2) S. John, *Phys. Rev. Lett.*, **58**, 2486 (1987).

(3) J. D. Joannopoulous, R. D. Meade, and J. N. Winn, *Photonic Crystals*, Princeton University Press, New York, 1995.

(4) S. Y. Lin, E. Chow, V. Hietala, P. R. Villeneuve, and J. D. Joannopoulous, *Science*, **282**, 274 (1998).

(5) M. Campbell, D. N. Sharp, M. T. Harrision, R. G. Denning, and A. J. Turberfield, *Nature*, **404**, 53 (2000).

(6) V. P. Tondiglia, L. V. Natarajan, R. L. Sutherland, D. Tomlin, and T. J. Bunning, *Adv. Mater.*, **14**, 187 (2002).

.(7) M. Mucha, *Prog. Polym. Sci.*, **28**, 837 (2003).

(8) T. J. Bunning, L. V. Natarajan, V. P. Tondiglia, G. Dougherty, and R. L. Sutherland, *J. Polym. Sci.; Part B: Polym. Phys.*, **35**, 2825 (1997).

(9) T. J. Bunning, L. V. Natarajan, V. P. Tondiglia, and R. L. Sutherland, *Annu. Rev. Mater. Sci.*, **30**, 83 (2000).

(10) M. D. Sarkar, N. L. Gill, J. B. Whitehead, and G. P. Crawford, *Macromolecules*, **36**, 630 (2003).

(11) T. Kyu, N. Domasius, and H.-W. Chiu, *Phys. Rev. E*, **63**, 061802 (2001).

(12) R. L. Sutherland, V. P. Tondiglia, L. V. Natarajan, and T. J. Bunning, *J. Appl. Phys.*, **96**, 951 (2004).

(13) S. Meng, T. Kyu, L. V. Natarajan, V. P. Tondiglia, R. L. Sutherland, and T. J. Bunning, *Macromolecules*, **38**, 4844 (2005).

(14) P. J. Flory, *J. Chem. Phys.*, **10**, 51 (1942).

(15) M. L. Huggins, *J. Phys. Chem.*, **46**, 151 (1942).

(16) W. Maier and A. Z. Saupe, *Naturforsch.*, **13a**, 564 (1958).

(17) J. D. Gunton, M. San Miguel, and P. S. Sahni, *Phase Transitions and Critical Phenomena*, Academic Press, New York, 1983.

(18) S. Meng, K. Nanjundiah, T. Kyu, L. V. Natarajan, V. P. Tondiglia, and T. J. Bunning, *Macromolecules*, **37**, 3792 (2004).

(19) C. Shen and T. Kyu, *J. Chem. Phys.*, **102**, 556 (1995).

(20) K. Nanjundiah, Master's Thesis, The University of Akron, 2003.

(21) K. Dusek, *J. Polym. Sci.; Part C: Polym. Symp.*, **16**, 1289 (1967); K. Dusek and W. Prins, *Adv. Polym. Sci.*, **6**, 1 (1969).

(22) H. M. J Boots, C. Kloosterboer, C. Serbutoviez, and F. J. Touwslager, *Macromolecules*, **29**, 7683 (1996).

(23) P. J. Flory and B. Erman, *Macromolecules*, **15**, 800 (1982).

(24) G. R. Yandek, Ph. D. Dissertation, The University of Akron, 2005.

(25) R. L. Sutherland, V. P. Tondiglia, L. V. Natarajan, and T. J. Bunning, *Appl. Phys. Lett.*, **79**, 1420 (2001).